Chinese Chemical Letters 34 (2023) 108446

Contents lists available at ScienceDirect

Chinese Chemical Letters

journal homepage: www.elsevier.com/locate/cclet

Manipulation of the PdAu–$PdAuO_x$ interface on Pd-Au bimetallic catalysts for the direct synthesis of hydrogen peroxide

Jixuan Zhang[a], Pengfei Tian[b], Aihao Xu[c], Like Ouyang[d], Zixu Yang[a,*], Jing Xu[a,c,*]

[a] State Key Laboratory of Chemical Engineering, School of Chemical Engineering, East China University of Science and Technology, Shanghai 200237, China
[b] Key Laboratory of Pressure Systems and Safety, Ministry of Education, East China University of Science and Technology, Shanghai 200237, China
[c] Guangxi Key Laboratory of Petrochemical Resource Processing and Process Intensification Technology, School of Chemistry and Chemical Engineering, Guangxi University, Nanning 530004, China
[d] College of Chemical Engineering, Sichuan University, Chengdu 610065, China

ARTICLE INFO

Article history:
Received 27 January 2023
Revised 9 April 2023
Accepted 11 April 2023
Available online 13 April 2023

Keywords:
H_2O_2 synthesis
Bimetallic catalysts
Palladium particle size
Pd^0/Pd^{2+} ratio
Structure-performance relationship

ABSTRACT

Direct synthesis of H_2O_2 from H_2 and O_2 *via* heterogeneous catalysis is an environmentally friendly and atomically economic alternative to the traditional anthraquinone oxidation (AO) process. Optimizing the electronic and geometric structures of the active metals to break the current limitations of hydrogenation rate and H_2O_2 selectivity is a promising and challenging topic. In this study, a series of Pd-Au bimetallic catalysts supported on TiO_2 with a metal loading of 3.0 wt% and a constant Pd/Au molar ratio (Pd:Au = 2:1) were prepared. The catalysts were reduced in H_2 at different temperatures (473, 573 and 673 K), and their catalytic activity for the direct H_2O_2 synthesis were evaluated at 283 K and 0.1 MPa. H_2 reduced Pd-Au catalysts exhibited superior performance in direct H_2O_2 synthesis. The maximum H_2O_2 selectivity of 87.7% and H_2O_2 yield of 3116.4 mmol h^{-1} $g_{Pd}{}^{-1}$ were achieved over the $Pd_{2.0}Au_{1.0}$-573 catalyst with a H_2 conversion of 12.8%. The tailored local chemical environment caused by H_2 reduction creates a balanced ratio of Pd^0 and PdO_x sites, thus improving the selectivity towards H_2O_2. This work developed an effective strategy for fabrication of highly active and stable Pd-based H_2O_2 synthesis catalysts with high H_2O_2 yield.

Hydrogen peroxide (H_2O_2), one of the 100 most important chemicals in the world, has been recognized as an efficient and green oxidant because of its numerous advantages such as mild reaction conditions, fast reaction speed, high selectivity and pollution-free. As a result, hydrogen peroxide is heavily used as a feedstock or additive (*e.g.*, oxidant [1,2], bleaching agent [3], disinfectant [4]) in a wide range of manufacturing sectors, such as chemicals [5], papermaking, textile [6], medicine [7], electronics, and environmental protection [8].

The anthraquinone oxidation (AO) has maintained its position as the most mature hydrogen peroxide synthesis technology since 1840s [9,10], and still accounts for more than 95% of the world's H_2O_2 production today. Despite the high H_2O_2 yield per cycle, the AO process also suffers from the complicated process, side reactions that lead to a considerable consumption of alkyl anthraquinone, rapid deactivation of hydrogenation catalyst and high separation cost [11]. Furthermore, this process is only profitable on a large-scale production ($>4 \times 10^4$ t/a) [12,13]. Given the existing issues in AO process, the direct synthesis of hydrogen peroxide from H_2 and O_2 over heterogeneous catalysts offers an attractive and green alternative process, which was first introduced in 1914 [14]. However, the process has not been commercialized yet due to the strong explosive potential of the mixture of H_2 and O_2 at high pressures, as well as the low productivity caused by the side reactions, such as hydrogenation and degradation of H_2O_2 in the process.

The high activity and selectivity of Pd-based catalysts for direct synthesis of H_2O_2 is well known and has received great attention for decades [15]. Recent studies have highlighted the enhanced H_2O_2 selectivity by alloying Pd with a secondary metal such as Au. The latter is often attributed to the geometrical effect, which gives emphasis on the advantage of Pd monomers surrounded by Au atoms towards H_2O_2 formation, while contiguous Pd ensembles are more favorable for H_2O_2 hydrogenation [16,17]. As H_2O_2 synthesis over Pd-based bimetallic catalysts is a surface-catalyzed and structure-sensitive reaction, modification of catalyst surface composition *via* surface pretreatment may alter the chemical environment of active sites and the product selectivity.

* Corresponding authors at: State Key Laboratory of Chemical Engineering, School of Chemical Engineering, East China University of Science and Technology, Shanghai 200237, China.
E-mail addresses: zixu.yang@ecust.edu.cn (Z. Yang), xujing@ecust.edu.cn (J. Xu).

https://doi.org/10.1016/j.cclet.2023.108446
1001-8417/

Table 1
Performance of $Pd_{2.0}Au_{1.0}/TiO_2$ catalysts with different heat treatment temperature.[a]

Catalyst	H_2 conversion (%)	H_2O_2 selectivity (%)	H_2O_2 productivity (mmol h^{-1} $g_{Pd}{}^{-1}$)	TOF (h^{-1})
$Pd_{2.0}Au_{1.0}$-0	12.0	71.8	2072.5	555.3
$Pd_{2.0}Au_{1.0}$-473	17.7	73.0	3116.4	1103.3
$Pd_{2.0}Au_{1.0}$-573	12.8	87.7	2696.6	1006.3
$Pd_{2.0}Au_{1.0}$-673	8.1	81.3	1589.3	638.7

[a] Reaction conditions: 50 mg catalyst, 60 mL ethanol with 0.38 mL H_2SO_4 as a solvent, a total gas flow rate of 60 mL/min ($H_2/O_2/N_2 = 15/60/25$), 283 K, atmospheric pressure, stirring rate 1000 rpm, 1/6 h.

For selective H_2 oxidation on Pd catalysts, there are discrepancies regarding the active phases since the copresence of metal Pd (Pd^0) and Pd oxide (PdO_x) in the reaction system. For example, Gudarzi *et al*. reported that PdO(II) species showed a higher selectivity towards H_2O_2 than Pd^0 in both mono Pd [18] and bimetallic Pd-Au [19] catalysts. The lower H_2O_2 selectivity on Pd^0 was attributed to the reabsorption and the subsequent degradation of H_2O_2 on Pd^0 surface according to Choudhary [20–25]. Contrarily, some studies reported higher conversion and selectivity toward H_2O_2 on partially reduced PdO_x species [26–28]. Recently, *N*-heterocyclic carbenes (NHC) was adopted as electronic modifiers of Pd, and the optimized catalyst with an appropriate surface Pd^0/Pd^{2+} ratio yielded twice as much H_2O_2 formation rate as the unmodified counterpart [29].

In Pd catalyzed H_2O_2 synthesis reaction, the chemical composition (*e.g.*, Pd^0/Pd^{2+} molar ratio) or particle size of the Pd species can be finely tuned during the calcination of the precursor and the pretreatment prior to reaction [30,31]. Calcination under prolonged duration or elevated temperature was found to result in an increase in the fraction of Pd^{2+} to formation of a surface oxide layer [32], and hence a decreased H_2O_2 formation rate [33]. But on the other hand, the increasing calcination temperature will undoubtedly be accompanied by a growing average crystallite size [34,35] and an affected H_2O_2 selectivity. More recently, Hang *et al*. reported a Pd/C catalyst calcined at 523 K showing a promising H_2O_2 productivity of 4443 mmol h^{-1} $g_{Pd}{}^{-1}$ with 94.5% selectivity [36]. The enhanced catalytic performance was attributed to the formation of small and highly oxidized Pd NPs (1.4–2.5 nm). Similarly, Pritchard observed that a mild heat treatment at 575 K was capable of forming an optimal Pd^0/Pd^{2+} ratio without causing a significant growth of particle size [37]. Simon *et al*. successfully encapsulated small Pd-rich NPs in the amorphous SnO_x layer through an oxidation-reduction-oxidation (O-R-O) heat treatment cycle, which prevents the sequential hydrogenation and degradation of H_2O_2 [38].

In our previous work, we have known that small Pd NPs (particle size of 1.4–2.5 nm) and exposure of active sites at Pd^0/PdO interfaces are important parameters enhancing H_2O_2 selectivity over Pd catalysts [39,40]. We also demonstrated that alloying Pd with appropriate amount of Au effectively reduced the quantity of contiguous Pd ensembles, thus inhibiting the degradation of H_2O_2 *via* hydrogenation pathway. The highest H_2O_2 selectivity of 48.1% was achieved with an optimal Pd/Au ratio of 2.0 and total metal content of 3.0 wt% [41]. On the basis of our previous studies on direct synthesis of H_2O_2 over Pd-based catalysts (Table S1 in Supporting information), this study demonstrated that catalyst calcination and pretreatment protocol had great impacts on the morphology and chemical composition of Pd NPs, and ultimately on catalytic performance with regard to selectivity and productivity of H_2O_2.

The four catalyst samples were prepared and tested for their capability to catalyze the direct synthesis of H_2O_2 under atmospheric pressure. A prior blank experiment was used to exclude the catalytic activity from the support. Detailed catalyst preparation, characterization and testing methods are available in Supporting information. Since the formation of H_2O_2 always occurs with its hydrogenation/decomposition reactions, the H_2O_2 productivity is reported as its net formation rate [42]. Table 1 shows that H_2O_2 selectivity of unreduced catalyst remains 71.8%, but increases abruptly to 87.7% after reduction under 573 K. A further increase of reduction temperature to 673 K leads to a slight decrease in H_2O_2 selectivity. It is also noticed that catalysts reduced at mild temperatures (473 K and 573 K) exhibit higher H_2 conversion than the unreduced catalyst. Higher temperature reduction tends to trigger the sintering of the metal NPs, which may cause the reduction in the number of active sites as well as the activity loss. This is verified by the abrupt decrease in H_2 conversion when the reduction temperature increases to 673 K. A similar trend was observed for the H_2O_2 productivity as well. The highest H_2O_2 productivity was obtained with $Pd_{2.0}Au_{1.0}$-473 (3116.4 mmol h^{-1} $g_{Pd}{}^{-1}$), which also exhibited the highest H_2 conversion (17.7%). By evaluating the dispersion of metal atoms exposed to reactants based on a hemispheric model, we also calculated the turnover frequency (TOF, h^{-1}), which showed a similar trend with the productivities. The TOFs of the reduced catalysts were generally higher than that of the unreduced one, with a highest value of 1103.3 h^{-1} occurring on the catalysts reduced at the lowest temperature (473 K). And then, it showed a slight decrease after the first additional 100 K, but when it came to another same magnitude of temperature increase, it responded with a rapid decline of more than 30%.

The impacts of H_2 reduction pretreatment on decomposition/hydrogenation side reactions of H_2O_2 were also studied. Fig. S1 (Supporting information) shows that the H_2O_2 concentration barely changes within 60 min under pure N_2 flow, indicating no activity for H_2O_2 decomposition, which agrees with our previous studies [41]. When switching the gas feed from N_2 to $15H_2/85N_2$, a significant drop in H_2O_2 concentration was observed for all catalysts. Higher reduction temperature results in a faster H_2O_2 hydrogenation rate, which matches the growth of the average particle size measured by TEM (Fig. 1) which will be discussed in the next section. The enhanced hydrogenation activity on large Pd NPs is due to the fact that the cleavage of O-O bond is favored on the extended Pd^0 ensembles. To sum up, the hydrogenation side reaction is the primary cause affecting the selectivity and net productivity of H_2O_2 during direct H_2O_2 synthesis from H_2 and O_2.

The discrepancies in catalytic performance seen for Pd-Au catalysts with the same nominal composition but different reduction procedures encourage us to examine the surface/bulk structure and chemical composition of the catalysts for better understanding of the structure-performance relationship.

Fig. 1 shows the TEM images of the Pd-Au bimetallic catalysts, as well as the corresponding particle size distribution of the Pd particles. It can be seen that the TiO_2 particles exhibit the same morphology after reduction pretreatment under different temperatures with an average particle size of 25 nm, suggesting that reduction treatment does not lead to obvious agglomeration of TiO_2 support. Pd NPs with different dimensions, ranging from small clusters of several atoms (<1 nm) to large Pd-Au particles (>10 nm), were clearly visualized on the images. Reduction pretreatment results in an abrupt increase in average Pd particle size from 2.8 ± 0.7 nm to 3.7 ± 0.8 nm. Increasing reduction temperature from 473 K to

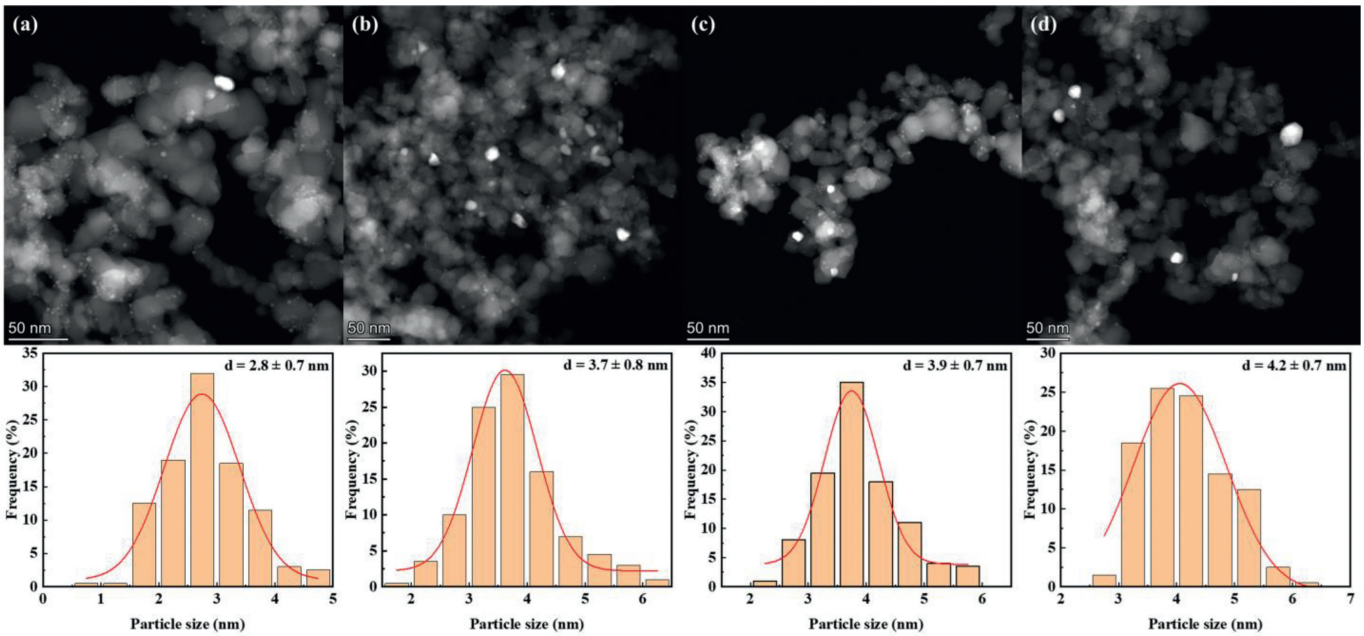

Fig. 1. TEM images and Pd particle sizes of the fresh catalysts. (a) $Pd_{2.0}Au_{1.0}$-0, (b) $Pd_{2.0}Au_{1.0}$-473, (c) $Pd_{2.0}Au_{1.0}$-573, (d) $Pd_{2.0}Au_{1.0}$-673.

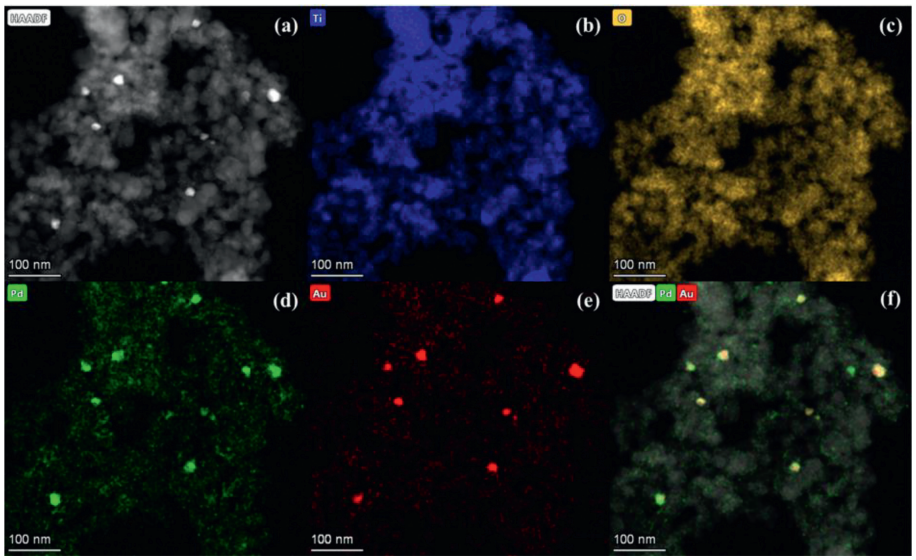

Fig. 2. Microstructure analysis of $Pd_{2.0}Au_{1.0}/TiO_2$ catalysts. (a) STEM-HAADF grayscale image of $Pd_{2.0}Au_{1.0}/TiO_2$, (b-f) STEM-EDS maps of $Pd_{2.0}Au_{1.0}/TiO_2$. Elements shown in blue, yellow, green and red refer to Ti, O, Pd and Au, respectively.

673 K causes a moderate growth on the average particle size from 3.7 ± 0.8 nm to 4.2 ± 0.7 nm, equivalent to a growth rate of *ca.* 0.2–0.3 nm per 100 K. Analysis of the TEM images and particle size distribution indicate that reduction treatment under mild temepratures causes the agglomeration of metal NPs to some extent.

High-angle annular dark-field scanning transmission electron microscopy (HAADF-STEM) was used to analyze the micromorphology and the elemental distribution of Au and Pd (Fig. 2). The distributions of both Pd and Au are almost overlapped with that of Ti and O, confirming the homogeneity of the supported catalyst in the form of Pd-Au bimetallic particles. In the same figure, it can also be seen that the spatial distribution of aggregated forms of Au is highly consistent with that of large Pd NPs with a size of 10–15 nm, suggesting the presence of highly-enriched large particles in addition to the other highly-dispersed ones. The energy-dispersive X-ray spectroscopy (EDS) elemental mapping images confirmed a uniform distribution of Pd and Au in the bimetallic particles and the tight contact between the two metals. The hybrid support was also identified by the elemental mapping of Ti and O, as shown in Figs. 2b and c, respectively. The XRD patterns (Fig. 3a) of the both unreduced and reduced Pd-Au bimetallic catalysts reveal both characteristics of rutile (25.3°, 37.8° and 48.0°) and anatase phases (27.4°, 36.1° and 54.3°, Degussa P25) with identical 2θ positions, manifesting that the crystal structure of the TiO_2 support is intact during reduction pretreatment [43]. Pd shows a weak signal belonging to Pd (111) at $2\theta = 40.1°$ in $Pd_{2.0}Au_{1.0}$-673 [44], whereas the diffraction peaks of Au are absent, presumably owing to the low metal loading and high metal dispersion. Such cases are not rare in palladium-based catalysts prepared by similar impregnation method [31]. Nevertheless, all catalysts are consisted of mainly small metal particles, in good agreement with the TEM results.

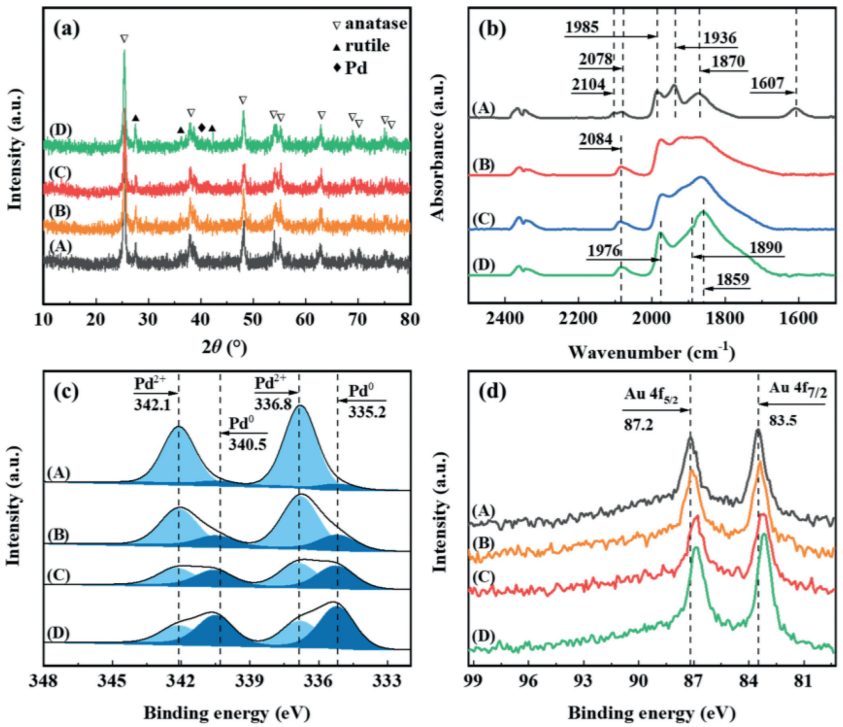

Fig. 3. (a) XRD patterns, (b) CO-DRIFTS, (c) fitting Pd 3d XPS spectra, and (d) Au 4f XPS spectra of $Pd_{2.0}Au_{1.0}/TiO_2$ catalysts with different heat treatment temperature: (A) $Pd_{2.0}Au_{1.0}$-0, (B) $Pd_{2.0}Au_{1.0}$-473, (C) $Pd_{2.0}Au_{1.0}$-573, (D) $Pd_{2.0}Au_{1.0}$-673.

The surface characteristics of Pd-Au bimetallic catalysts after reduction treatment was studied using CO-DRIFTS, and the observed spectra were displayed in Fig. 3b. CO absorption bands located ~1800–2100 cm^{-1} were observed in all catalysts, which were attributed to CO adsorbed on metallic Pd atoms with different bonds (*e.g.*, linear, bridged, and hollow). No CO adsorption bands on Au (*ca.* 2100 cm^{-1}) was observed [45]. The peak at 2084 cm^{-1} (peak 1) associated with the linearly bonded CO (Pd-CO) on Pd atoms of low coordination, *e.g.*, corner or edge sites [46] is visible for all reduced catalysts, and this peak splits into two small peaks located at 2104 and 2078 cm^{-1} for the unreduced catalyst [47]. The three successive peaks at 1985, 1936, and 1870 cm^{-1} (peak 2) were assigned to chemisorbed CO on bridged- and multi-folded hollow Pd^0 sites [48].

More intriguingly, the bands related to CO adsorbed on these Pd^0 sites grow sharper upon increasing reduction temperature. The peak area ratio of the CO_{linear} bands *vs.* $CO_{bridged} + CO_{hollow}$ bands was decreased regularly from 0.059 to 0.025 (Table S2 in Supporting information), indicating that higher reduction pretreatment results in the exposure of more flat sites with continuous Pd ensembles. These features also shifted slightly to lower wavenumbers with increasing reduction temperatures, and eventually ended at 1976, 1890 and 1859 cm^{-1} in the case of $Pd_{2.0}Au_{1.0}$-673. These redshifts may be attributed to a stronger electronic back-donation from the d orbital of Pd metal to the 2π molecular orbitals of CO molecules, indicating a remarkable enhancement in the d orbital electron density from the increase in Pd^0 [49,50]. Moreover, a small band around 1607 cm^{-1} on $Pd_{2.0}Au_{1.0}$-0 corresponding to surface carbonate species was absent in the spectra of the reduced catalysts presumably because the carbonate species were removed after reduction treatment.

In Pd-catalyzed direct H_2O_2 synthesis, Pd^0 is considered as responsible for H_2 dissociation while PdO is suggested to activate O_2 associatively. A balanced ratio of Pd^0/Pd^{2+} is necessary for high H_2O_2 yield. Herein, the chemical states of the supported Pd NPs were studied *via* XPS survey of Pd 3d spectra, and the results were shown in Fig. 3c and Table 2. The curve-fitting of Pd 3d spectra show Pd^0 (335.2 and 340.5 eV) and Pd^{2+} (336.8 and 342.1 eV) components for all catalyst samples [51,52]. The molar ratio of Pd^0/Pd^{2+} increases steadily along with the rising reduction temperature, from 0.1 in the unreduced catalyst to 1.6 in $Pd_{2.0}Au_{1.0}$-673. The increased surface molar ratio of Pd^0/Pd^{2+} after H_2 reduction treatment provides more sites for H_2 dissociation, thus resulting in a faster hydrogenation rate, as observed in $Pd_{2.0}Au_{1.0}$-473 [53,54]. However, excessive Pd^0 would lead to a decrease in the $PdAu\text{-}PdAuO_x$ interface sites as well as an increase in metallic Pd sites, which is more feasible for the breakage of O-O bond in O_2, as evidenced by theoretical calculation (Fig. S2 in Supporting information). The rising reduction temperature also leads to an adverse aggregation of both surface Pd and Au atoms, resulting in the gradual destruction of the high dispersion, which may dominate the downward catalyst performance, manifested as an even lower H_2O_2 productivity than the untreated catalysts when the reduction temperature reaches 673 K.

For XPS Au 4f (Fig. 3d), the Au $4f_{5/2}$ and Au $4f_{7/2}$ BE peaks appeared at 87.2 eV and 83.5 eV, respectively, lower than those of naturally occurring metallic Au (BE 87.7 and 84.0 eV [55]) by 0.5 eV. This can be partly ascribed to the quantum size effect, which implies that the nano-sized Au particles have more surface atoms than bulk Au, resulting in a shift of the d-band towards Fermi level [56], as well as the electron transfer from Au^0 to both Pd^0 [57] and TiO_2 [58]. Upon increasing reduction temperature, the Au 4f peaks are further negatively shifted. It implies that high temperature reduction results in an increase in the electron density of Au.

To get more insights on the effects of surface chemical composition on the adsorption behaviors of the Pd catalysts, O_2- and H_2-TPD studies were carried out and the results were shown in Figs. 4a and b, respectively. Two desorption peaks at 365 K and 447 K were detected for all catalysts, mainly attributed to the adsorption of O_2 molecules on oxygen vacancies of surface TiO_2 and Pd particles [59], respectively. The strong O_2 desorption peaks observed in the high temperature region of 850–950 K can be attributed to

Table 2
The quantified XPS data of the surface Pd atoms.

Catalyst	Pd species	$3d_{5/2}$		$3d_{3/2}$		Pd^0/Pd^{2+}
		BE (eV)	FWHM (eV)	BE (eV)	FWHM (eV)	
$Pd_{2.0}Au_{1.0}$-0	Pd^0	335.2	2.0	340.5	2.0	0.1
	Pd^{2+}	336.8	1.7	342.1	1.7	
$Pd_{2.0}Au_{1.0}$-473	Pd^0	335.2	2.0	340.5	2.0	0.3
	Pd^{2+}	336.8	2.0	342.1	2.0	
$Pd_{2.0}Au_{1.0}$-573	Pd^0	335.2	2.0	340.5	2.0	0.9
	Pd^{2+}	336.8	2.0	342.1	2.0	
$Pd_{2.0}Au_{1.0}$-673	Pd^0	335.2	1.9	340.5	1.9	1.6
	Pd^{2+}	336.8	2.0	342.1	2.0	

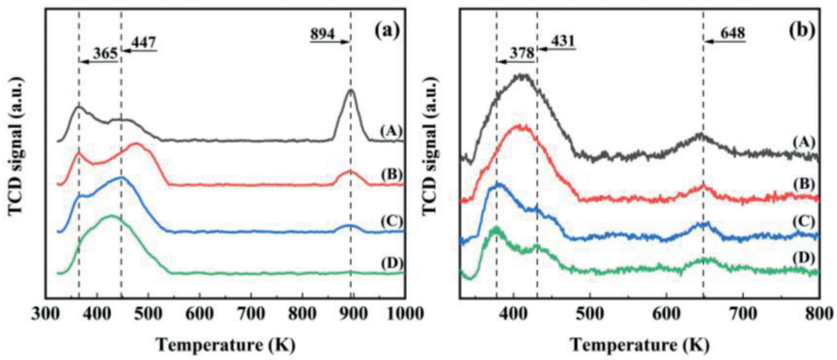

Fig. 4. (a) O_2-, (b) H_2-TPD profiles obtained for different catalysts in an Ar flow with a ramping rate of 10 K/min. (A) $Pd_{2.0}Au_{1.0}$-0, (B) $Pd_{2.0}Au_{1.0}$-473, (C) $Pd_{2.0}Au_{1.0}$-573, (D) $Pd_{2.0}Au_{1.0}$-673.

the decomposition of surface palladium oxide [60]. Upon rising reduction temperature, the molecular O_2 peaks on Pd particles gradually shifted to lower temperature with increased peak intensities. On the other hand, the high temperature O_2 desorption peak broadens and even flatten out in the $Pd_{2.0}Au_{1.0}$-673 sample, suggesting an increasing ratio of Pd^0/Pd^{2+}, which is in line with the XPS results. More importantly, it is known that the activated O_2 molecules are important for the outcome of the reaction, which means excessively strong adsorption may lead to oxygen dissociation while weak adsorption may lead to oxygen desorption from the catalyst surface. The 573 K reduced one seems to have the optimal adsorption strength, thus turning out with the highest H_2O_2 selectivity.

For H_2-TPD, all catalysts showed similar desorption profiles with two major desorption peaks, denoted as H_α (350–500 K) and H_β (620–670 K). The H_α peaks corresponding to the chemisorbed H_2 species desorption on metallic Pd sites contained two overlapped peaks. The peak centered at *ca.* 378 K was allocated to H_2 derived from β-hydride decomposition [61,62]; the peak centered at *ca.* 431 K can be attributed to the desorption of H_2 on isolated Pd^0 sites that have no interactions with Au [61,63]. The H_β peaks were probably due to the H_2 desorption from highly dispersed Pd atoms in Pd-Au particles. Increasing reduction temperature results in a decrease of H_α desorption amount. Such behavior implies a loss of metallic Pd sites which may be ascribed to the particle growth upon H_2 reduction under elevated temperatures.

A hydrogenation reaction pathway study in H_2O_2 synthesis on Pd catalysts through isotopic experiments evidenced an associative adsorption pathway for O_2 molecules [53], and the formation of OOH intermediate from the dissociated H atoms and activated O_2 molecules was considered as the key step for H_2O_2 synthesis [64]. Reaction pathway that leads to the dissociation of O_2 molecules tends to end up with H_2O as the main product. But the O-O bond cleavage, which was considered to be adverse for H_2O_2 formation, was significantly suppressed on Pd monomers surrounded by less active Au atoms [41,65]. Our previous study has already unraveled a Pd–PdO–TiO_2 interface where the Pd^0 atoms were most exposed on the upper layers of particles, and PdO species were present at the interface of Pd NPs and TiO_2 [40]. In this work, we adopted the modeled PuAu-PdAuOx interface as the active sites for H_2O_2 synthesis, where the upper metallic Pd species take responsibility for H_2 dissociated activation and the oxidized Pd species for O_2 non-dissociated activation. The reducible support TiO_2 was selected to better ensure the coexistence of metallic and oxidized metal components on the catalyst surface and the highly dispersed Au serves to stabilize the enrichment of metal Pd at the top of the particles. Single metallic or oxidized Pd species will lead to a dissatisfactory H_2O_2 productivity. Because the initial structure of the interface between PdAu and $PdAuO_x$ is very much dictated by the activation conditions, so as the particle size, the final catalytic performance will be completely different. These insights on the critical role of PdAu–$PdAuO_x$ interface in H_2O_2 synthesis inspired us to further refine the geometric and chemical properties of the interface for optimal H_2O_2 selectivity and yield by reduction pretreatment.

The reduction pretreatment on Pd-Au bimetallic catalysts obviously outperforms the unreduced one in terms of both H_2 conversion and H_2O_2 selectivity. The low H_2 conversion of the $Pd_{2.0}Au_{1.0}$-0 sample can be attributed to a lack of Pd^0 sites for H_2 dissociation, and the reduction of PdO_x by H_2 leads to a rapid accumulation of H_2O at the initial stage of the reaction, which undoubtedly compromises the average H_2O_2 selectivity. However, increasing reduction temperature not only leads to more Pd^0 for H_2 dissociation, but also to a growth in particle size caused by varying degrees of metal sintering, as observed in the TEM results. And the latter explains the dropping H_2 conversion from 17.7% to 8.1% with the increasing reduction temperature, along with the H_2O_2 productivity.

As mentioned above, H_2O_2 synthesis was primarily occurred on the PdAu–$PdAuO_x$ interface (Fig. 5a), the structure of which was affected by the reduction conditions. The surface Pd^0/Pd^{2+} ratio of the original $Pd_{2.0}Au_{1.0}/TiO_2$ increases from 0.1 to 0.3 (reduced at 473 K) and 0.9 (reduced at 573 K). The optimal Pd^0/Pd^{2+} ratio in

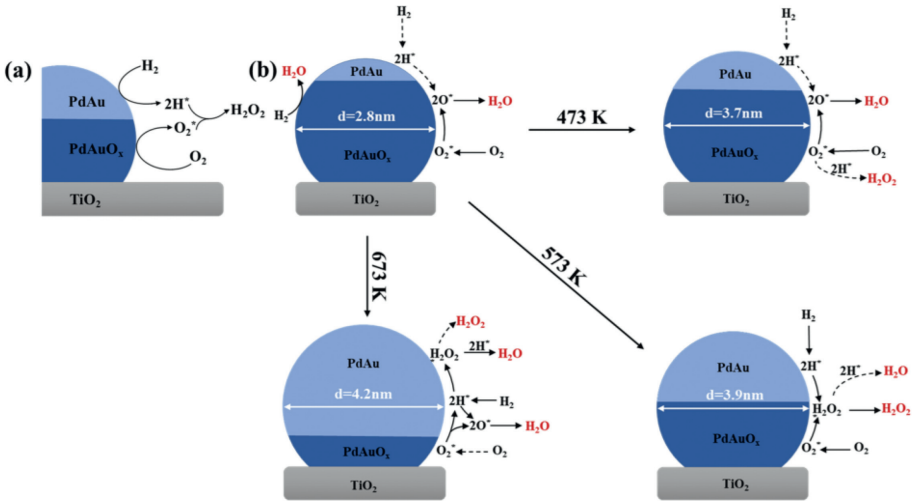

Fig. 5. (a) The proposed reaction mechanism of H_2O_2 synthesis on $Pd_{2.0}Au_{1.0}/TiO_2$ catalysts. (b) The possible change of structural model after reduction treatment.

the $Pd_{2.0}Au_{1.0}$-573 demonstrates the highest H_2O_2 selectivity due to the downward shift of the PdAu and $PdAuO_x$ interface demarcation line (Fig. 5b) to form the maximum active sites towards H_2O_2 synthesis. Nonetheless, a further increase in reduction temperature brings an opposite effect. We owe this to a combined effect: (I) The decreased PdAu–$PdAuO_x$ interface in step with the continues increased Pd^0/Pd^{2+} ratio, directly reduced the number of active sites; (II) The high rate of parallel side reaction caused by the uncontrollable particle size growth, for O_2 prefers to be dissociated on continuous Pd^0 sites; (III) The excessive tandem side reactions, as the hydrogenation tests have shown that contiguous Pd ensembles are more active for H_2O_2 hydrogenation than small Pd clusters [66].

Based on the discussion above, it can be summarized that the hydrogenation activity and H_2O_2 selectivity depends on the balance of the sites for hydrogenation and associative O_2 activation, and it is highly sensitive to the reduction conditions (*e.g.*, temperature). It should be also noted that the reduction temperature should be finely tuned to avoid the activity loss caused by the sintering of metal NPs.

In conclusion, we successfully demonstrated an engineering control on the chemical states and geometry of PdAu–$PdAuO_x$ interface in a bimetallic Pd-Au/TiO_2 catalyst through a facile reduction pretreatment method, and eventually identified 573 K as the optimum reduction temperature. The optimal Pd^0/Pd^{2+} ratio at about 0.9 observed in $Pd_{2.0}Au_{1.0}$-573 showed the highest H_2O_2 selectivity of 87.7% compared with the unmodified one (71.80%), which is able to locate the PdAu–$PdAuO_x$ interface closest to the largest diameter on the catalyst surface, thereby increasing the number of the exposed number of active sites despite particle agglomeration. The insights on valence and morphology effect on catalytic activity provides a feasible approach to improve the direct synthesis of H_2O_2 *via* the modification of the Pd active surface through pre-activation treatment.

Declaration of competing interest

We declare that we do not have any commercial or associative interest that represents a conflict of interest associated with the work submitted.

Acknowledgments

This work was supported by the National Natural Science Foundation of China (Nos. 91934302 and 22178110), the Dean/Opening Project of Guangxi Key Laboratory of Petrochemical Resource Processing and Process Intensification Technology (No. 2020K001) and the Project of the Department of Science and Technology of Sichuan Province (No. 2023YFQ0086).

Supplementary materials

Supplementary material associated with this article can be found, in the online version, at doi:10.1016/j.cclet.2023.108446.

References

[1] N.P. Jayaweera, A.E. Hall, A.A. Wilson, et al., Inorg. Chim. Acta 506 (2020) 119507.
[2] M. Hajjami, A. Ghorbani-Choghamarani, M.A. Zolfigol, F. Gholamian, Chin. Chem. Lett. 23 (2012) 1323–1326.
[3] R. Hage, A. Lienke, Angew. Chem. Int. Ed. 45 (2006) 206–222.
[4] A.R. Matin, S. Yousefzadeh, E. Ahmadi, et al., Food Chem. Toxicol. 116 (2018) 129–137.
[5] H.Y. Guo, J.C. Li, Y.L. Shang, Chin. Chem. Lett. 20 (2009) 1408–1410.
[6] A. Asghar, A.A. Abdul Raman, W.M.A. Wan Daud, J. Clean. Prod. 87 (2015) 826–838.
[7] T. Hadzic, N. Aykin-Burns, Y. Zhu, et al., Free Radic. Biol. Med. 48 (2010) 1024–1033.
[8] Z. Wei, H. Xu, Z. Lei, et al., Chin. Chem. Lett. 33 (2022) 920–925.
[9] E. Santacesaria, M.D. Serio, A. Russo, U. Leone, R. Velotti, Chem. Eng. Sci. 54 (1999) 2799–2806.
[10] X. Chen, J. Catal. 220 (2003) 254–257.
[11] T. Ishihara, Y. Ohura, S. Yoshida, et al., Appl. Catal. A: Gen. 291 (2005) 215–221.
[12] J.K. Edwards, G.J. Hutchings, Angew. Chem. Int. Ed. 47 (2008) 9192–9198.
[13] J.K. Edwards, S.J. Freakley, A.F. Carley, C.J. Kiely, G.J. Hutchings, Acc. Chem. Res. 47 (2014) 845–854.
[14] H. Henkel, W. Weber, Patent, US 1108752, 1914.
[15] V.R. Choudhary, C. Samanta, P. Jana, Ind. Eng. Chem. Res. 46 (2007) 3237–3242.
[16] J. Gong, Chem. Rev. 112 (2012) 2987–3054.
[17] F. Gao, D.W. Goodman, Chem. Soc. Rev. 41 (2012) 8009–8020.
[18] D. Gudarzi, W. Ratchananusorn, I. Turunen, T. Salmi, M. Heinonen, Top. Catal. 56 (2013) 527–539.
[19] D. Gudarzi, W. Ratchananusorn, I. Turunen, M. Heinonen, T. Salmi, Catal. Today 248 (2015) 58–68.
[20] C. Samanta, V.R. Choudhary, Catal. Commun. 8 (2007) 73–79.
[21] V.R. Choudhary, C. Samanta, T.V. Choudhary, Catal. Commun. 8 (2007) 1310–1316.
[22] C. Samanta, V.R. Choudhary, Appl. Catal. A: Gen. 326 (2007) 28–36.
[23] C. Samanta, V.R. Choudhary, Catal. Commun. 8 (2007) 2222–2228.
[24] C. Samanta, V.R. Choudhary, Chem. Eng. J. 136 (2008) 126–132.
[25] C. Samanta, V.R. Choudhary, Appl. Catal. A: Gen. 330 (2007) 23–32.
[26] V.V. Krishnan, A.G. Dokoutchaev, M.E. Thompson, J. Catal. 196 (2000) 366–374.
[27] R. Burch, P.R. Ellis, Appl. Catal. B: Environ. 42 (2003) 203–211.
[28] Q. Liu, K.K. Gath, J.C. Bauer, R.E. Schaak, J.H. Lunsford, Catal. Lett. 132 (2009) 342–348.
[29] R.J. Lewis, M. Koy, M. Macino, et al., J. Am. Chem. Soc. 144 (2022) 15431–15436.
[30] A.A. Herzing, A.F. Carley, J.K. Edwards, G.J. Hutchings, C.J. Kiely, Chem. Mater. 20 (2008) 1492–1501.

[31] Y. Yan, H. Li, Z. Lu, et al., Chin. Chem. Lett. 30 (2019) 1153–1156.
[32] S. Melada, R. Rioda, F. Menegazzo, F. Pinna, G. Strukul, J. Catal. 239 (2006) 422–430.
[33] J.K. Edwards, J. Pritchard, M. Piccinini, et al., J. Catal. 292 (2012) 227–238.
[34] A. Villa, K. Dumoleijn, C. Evangelisti, K. Moonen, L. Prati, RSC Adv. 8 (2018) 15202–15206.
[35] D.R. Fertal, M. Monai, L. Proaño, et al., Catal. Today 382 (2021) 120–129.
[36] V.T.T. Hang, Y.M. Chung, Korean J. Chem. Eng. 37 (2020) 65–71.
[37] J. Pritchard, M. Piccinini, R. Tiruvalam, et al., Catal. Sci. Technol. 3 (2013) 308–317.
[38] S.J. Freakley, Q. He, J.H. Harrhy, et al., Science 351 (2016) 965–968.
[39] P. Tian, L. Ouyang, X. Xu, et al., J. Catal. 349 (2017) 30–40.
[40] L. Ouyang, P.F. Tian, G.J. Da, et al., J. Catal. 321 (2015) 70–80.
[41] L. Ouyang, G.J. Da, P.F. Tian, et al., J. Catal. 311 (2014) 129–136.
[42] E. Ntainjua N, M. Piccinini, J.C. Pritchard, et al., ChemSusChem 2 (2009) 575–580.
[43] Y. Zhang, Z.R. Tang, X. Fu, Y.J. Xu, ACS Nano 4 (2010) 7303–7314.
[44] Q. Meng, X. Wang, M. Xiao, et al., Chin. Chem. Lett. 34 (2023) 107221.
[45] T. Ricciardulli, J.S. Adams, M. DeRidder, et al., J. Catal. 404 (2021) 661–678.
[46] J. Xu, L. Ouyang, W. Mao, et al., ACS Catal. 2 (2012) 261–269.
[47] F. Gao, Y. Wang, D.W. Goodman, J. Phys. Chem. C 113 (2009) 14993–15000.
[48] T. Lear, R. Marshall, J.A. Lopez-Sanchez, et al., J. Chem. Phys. 123 (2005) 174706.
[49] P. Hu, D.A. King, M.H. Lee, M.C. Payne, Chem. Phys. Lett. 246 (1995) 73–78.
[50] C. Lin, H. Pan, Z. Yang, et al., Ind. Eng. Chem. Res. 59 (2020) 6424–6434.
[51] E.H. Voogt, A.J.M. Mens, O.L.J. Gijzeman, J.W. Geus, Surf. Sci. 373 (1997) 210–220.
[52] F.P. Leisenberger, G. Koller, M. Sock, et al., Surf. Sci. 445 (2000) 380–393.
[53] J.H. Lunsford, J. Catal. 216 (2003) 455–460.
[54] S. Chinta, J. Catal. 225 (2004) 249–255.
[55] H.G. Boyen, G. Kastle, F. Weigl, et al., Science 297 (2002) 1533–1536.
[56] F.W. Chang, H.Y. Yu, L. Selva Roselin, H.C. Yang, Appl. Catal. A: Gen. 290 (2005) 138–147.
[57] R. Liu, Y. Yu, K. Yoshida, et al., J. Catal. 269 (2010) 191–200.
[58] R. Meyer, C. Lemire, S.K. Shaikhutdinov, H.J. Freund, Gold Bull. 37 (2004) 72–124.
[59] M.A. Henderson, W.S. Epling, C.L. Perkins, C.H.F. Peden, U. Diebold, J. Phys. Chem. B 103 (1999) 5328–5337.
[60] J.J.A. Hinojosa, H.H. Kan, J.F. Weaver, J. Phys. Chem. C 112 (2008) 8324–8331.
[61] V.H. Sandoval, C.E. Gigola, Appl. Catal. A: Gen. 148 (1996) 81–96.
[62] J. Lee, H. Rhee, J. Catal. 177 (1998) 208–216.
[63] P.J. Berlowitz, D.W. Goodman, Langmuir 4 (1988) 1091–1095.
[64] M.G. Seo, H.J. Kim, S.S. Han, K.Y. Lee, Catal. Surv. Asia 21 (2017) 1–12.
[65] H.C. Ham, G.S. Hwang, J. Han, S.W. Nam, T.H. Lim, J. Phys. Chem. C 113 (2009) 12943–12945.
[66] V.R. Choudhary, C. Samanta, T.V. Choudhary, Appl. Catal. A: Gen. 308 (2006) 128–133.